A PHYSIOLOGY-BASED PHARMACOKINETIC APPROACH TO CALCITRIOL QUANTUM DOT DISTRIBUTION FOR USE IN INFLAMMATORY BREAST CANCER TREATMENT

by

Margot Wagner

A thesis submitted to the Faculty of the University of Delaware in partial fulfillment of the requirements for the degree of Honors Degree in Chemical and Biomolecular Engineering with Distinction

Spring 2018

A PHYSIOLOGY-BASED PHARMACOKINETIC APPROACH TO CALCITRIOL QUANTUM DOT DISTRIBUTION FOR USE IN INFLAMMATORY BREAST CANCER TREATMENT

by

Margot Wagner

Approved: _____

Prasad Dhurjati, Ph.D.
Professor in charge of thesis on behalf of the Advisory Committee

Approved: _____

Anja Nohe, Ph.D.
Committee member from the Department of Biological Sciences

Approved: _____

Matthew DeCamp, Ph.D.
Committee member from the Board of Senior Thesis Readers

Approved: _____

Paul Laux, Ph.D.
Director, University Honors Program

ACKNOWLEDGMENTS

I would like to thank my family and friends for their continuous support in completing my thesis and making it through the Chemical Engineering curriculum. I would like to thank my dad for always believing that I can do anything and always reminding me that my life is what I want it to be, not what other people tell me it is supposed to be. He also is living proof that it is never too late to grow as a person. I would like to thank my mom for her continuous love and support without which I would not be here. Both my parents helped me get through some of the most stressful and difficult times. I would like to thank my siblings for always being there for me and believing in me. I would like to thank my friends for listening to me complain and convincing me to have fun every once and a while.

I would like to thank Professor Dhurjati for inspiring me. Without him, I would not have done a senior thesis and would not be attending graduate school next year. Professor Dhurjati reminded me why I was here. He has been a wonderful mentor, showing me that you can do anything in any field you are interested in as long as you have drive and motivation.

I would like to thank Jon Gorky for helping me through this project with all my late-night questions and with reeling in the lovely Professor Dhurjati. I am sure he will continue to do amazing things.

Lastly, I would like to thank Professor Nohe for being here today and opening her research up to me. I would like to thank Professor DeCamp and my third reader group for their guidance and assistance.

TABLE OF CONTENTS

LIST OF TABLES

LIST OF FIGURES

ABSTRACT

Inflammatory breast cancer (IBC) is a rare yet aggressive form of breast cancer accounting for 1-5% of breast cancer cases. Due to its typically delayed diagnosis and highly metastatic nature, IBC has the lowest overall survival rate compared to other forms of breast cancer. Current treatment uses an aggressive multi-targeting approach but is still not very successful. Recent studies have indicated that calcitriol, the active form of vitamin D, has beneficial effects again SUM149 IBC cell proliferation, migration, and differentiation. Calcitriol can be conjugated with quantum dots (QDs) to allow for live cell direct imaging. Furthermore, IBC targeting methods utilizing SM3 have been demonstrated as effective which provide a method to target calcitriol directly to tumors while also monitoring QD levels. Here, a top-down physiology-based pharmacokinetic model was constructed and demonstrated as a method to augment *in vitro* and *in vivo* testing to provide additional simulated information on the behavior of QD treatment strategies for use in IBC. Overall, we were able to construct an effective model to describe the system in question and found results consistent with experimental studies of similar systems. Further *in vitro* studies would allow for replacement of some currently estimated parameters with biologically relevant ones.

Chapter 1

INTRODUCTION

1.1 Biological Background

1.1.1 Inflammatory Breast Cancer

Inflammatory breast cancer (IBC) is a rare yet aggressive form of breast cancer. While it only accounts for 1-5% of all breast cancer cases, it is met with a grim prognosis having the lowest overall survival rate compared to other breast cancers [1, 2]. Treatment plans consisting of only surgery or surgery and localized radiation therapy resulted in a less than 5% survival rate beyond 5 years, with a median survival time of less than 15 months and recurrence rates as high as 50% [2]. Utilizing current multiple-targeting approaches, IBC still only has 5- and 10-year disease-free survival rates of less than 45% and 20% respectively, which are lower than all other breast cancers [3]. IBC is a rapidly progressing and highly metastatic disease with a younger age of onset relative to other types of breast cancer with an average age of 55 years old for women [2]. It results from invasive ductal carcinomas which develop from the cells that line the lactation ducts of the breast and can disseminate throughout the rest of the body via dermal lymphatics as tumor emboli leading to both local and distant metastases [1]. When diagnosed with IBC, almost all women are lymph node positive and approximately one-third have gross distant metastasis [3]. The cancer is usually at stage III or IV when diagnosed, meaning that it has already begun spreading and metastasizing. Early symptoms include erythema (redness) and edema (swelling)

caused by IBC tumors blocking lymph drainage. These symptoms have been problematic because such inflammatory changes resemble an infection or rash leading to IBC often being misdiagnosed as mastitis or generalized dermatitis which delays treatment plans [1, 2].

Current treatment involves a multiple-targeting approach due to the aggressive nature of IBC. Unlike many other cancers, IBC cannot be treated by hormone treatment due to approximately one-third of IBC tumors being triple negative, meaning they do not produce estrogen, progesterone, and HER-2 receptors [1, 4]. Instead, current treatment plans involve systemic chemotherapy followed by radical mastectomy to remove the tumor and surrounding tissue and finally localized radiation therapy [3]. Despite this aggressive treatment plan, prognosis for IBC patients is poor, as alluded to previously. Researchers are now hoping to find new methods that are less aggressive and more efficient for the treatment of IBC. An ideal treatment method for IBC would be one that could prevent cell migration as well as preventing or disrupting the formation of emboli [4].

1.1.2 Calcitriol and Its Use in Therapies

A potential new therapeutic is the active form of Vitamin D, calcitriol, the majority of which is endogenously obtained by skin exposure to short wavelength ultraviolet light (UVB). This exposure takes the circulating inactive form of vitamin D and metabolizes it into calcidiol in the liver and further into calcitriol, the most biologically active metabolite of vitamin D, in the kidney [5]. Calcitriol is known to modulate calcium and phosphate homeostasis to maintain bone health [6]. It is the most biologically active in tissues positive for Vitamin D Receptors (VDR) including

organs such as the kidney, intestines, bone, or parathyroid gland [5]. Recently, vitamin D has been demonstrated to be a regulator of breast cancer cell proliferation, invasion, migration, differentiation, and apoptosis *in vitro.* Specifically, calcitriol has anti-proliferative effects on MCF-7 and SUM159 breast cancer cells. This is thought to be a result of calcitriol blocking the mitogenic effects of insulin-like growth factor I (IGF-I) through down-regulation of its receptors resulting in the G1 phase of the cell cycle pausing. As a result, a decrease in proliferation and increase in apoptosis is observed with the use of calcitriol [3].

Due to the promising results from the use of calcitriol in other breast cancers, research was done to observe the effects of using calcitriol for the treatment of inflammatory breast cancer, specifically the effects of calcitriol of SUM149 IBC cells. It was found that SUM149 cells exposed to calcitriol exhibited a decreased ability to migrate and invade; deceased ability to form tumor emboli and those that did form were smaller; and decreased metastasis. These results provide a hopeful path for clinical treatment of IBC [3]. Unfortunately, a major issue associated with calcitriol treatment is dosing. While calcitriol does have beneficial effects against SUM149 IBC cell lines, high concentrations are required which leads to serious unwanted side effects. Current research shows that dosing at 0.25 μg is safe while higher levels at 0.50 μg leads to hypercalcemia. Additionally, healthy calcitriol serum levels are below 50 pg/mL (0.12 nM) with higher levels resulting in similar hypercalcemia [4]. Therefore, targeting methods are required to reach desired levels of calcitriol at treatment sites without having an excess of calcitriol in the rest of the body.

1.1.3 Calcitriol Quantum Dots

Quantum dots (QDs) are semiconductor nanoparticles which can be used for fluorescent imaging under UV light. QDs exhibit high photostability and brightness as well as a narrow range of emission which make them desirable for fluorescent microscopic imaging. Additionally, they are available in a variety of shapes and sizes and have surface chemistries that are compatible with the aqueous environments of living cells [4]. While there is some concern with QDs being potentially toxic due to their cadmium core, the ones used in the study we will be referring to have a stable cadmium selenide (CdSe) core with a zinc sulfide shell coated in non-toxic polymer carboxyl groups [7]. Recent studies have shown no toxic side effects in monkeys due to CdSe QDs after 3 months to 1 year [4]. Quantum dots conjugated to calcitriol can be used to examine the distribution of calcitriol both *in vitro* and *in vivo* [4, 7].

To use calcitriol quantum dots for imaging, QDs are conjugated to calcitriol using an esterification reaction between a carboxyl group on the coating of the QDs and a hydroxyl group on the calcitriol to produce calcitriol quantum dots (CalQDs) which can then be used for live cell direct imaging [4]. To avoid hypercalcemia and potential toxicity from too much calcitriol, these CalQDs can be manipulated to target tumor sites allowing for a more effective treatment of IBC.

1.1.4 Targeted Calcitriol Quantum Dots

Mucin-1 (MUC1) is a glycoprotein that is expressed on the apical surface of epithelial cells. In IBC, MUC1 expression increases compared to other breast cancers where expression either decreases or is lost completely. Specifically, IBC overexpresses a hypoglycosylated form of MUC1. A potential option for targeting is

to utilize an SM3 clone of MUC1, which is a monoclonal antibody that recognizes hypoglycosylated MUC1 on breast carcinomas. Recently, Schaefer et. al have put forward a therapeutic method conjugating the SM3 clone of MUC1 antibodies with calcitriol quantum dots (SM3 CalQDs). These SM3 CalQDs can be used to target MUC1 overexpressing IBC cells, identify localization of IBC emboli, and act as a vehicle to administer calcitriol directly to affected areas to avoid hypercalcemia and other negative side effects. In their study, Schaefer et. al showed that SM3 CalQDs accumulate in tumor tissues and are taken up at a higher concentration than the control QDs (ConQDs) and CalQDs [4]. This provides a hopeful new therapeutic method for treating IBC at a clinical level. To better elucidate the details of the distribution of SM3 CalQDs as well as finding an adequate dosing regimen, we look to create a model here for the distribution of SM3 CalQDs in the human body.

1.2 Computational Background

1.2.1 Mathematical Modeling in Biological Sciences

The traditional approach to drug discovery involves bottom-up science whereby compounds are first studied to understand their interaction with drug targets followed by *in vitro* and *in vivo* animal lab testing with the drug eventually being tested in patients. Recent increases in mathematical modeling in drug discovery allows for a top-down mechanism to augment *in vitro* experimentation for studying and better understanding the effects of drugs in their environments. Use of simulations allows for more information to be obtained quicker and cheaper than biological trial and error methodology alone. With the increase in processing power provided by modern day

computers, more complex models are able to be handled that were previously mathematically intractable resulting in an exponential increase in this field. Interest in mathematical modeling in pharmacology first arose once legislation required pharmaceutical companies to establish standards and regulations for demonstrating the pharmacokinetics (PK; what the body does to the drug) and pharmacodynamics (PD; what the drug does to the body) of the drugs they produced and sold [8].

Mathematical models used describe the physical principles of the drug behavior with use of equations. Deterministic models are created and simulated on a computer to represent the interactions of a drug from the top-down based on preexisting known physicochemical information of that drug. These systems have input and output in the form of stimuli and responses and look at the properties of processes to gain better understanding of the biological system as a whole. When used diagnostically, the goals of these models are multifaceted, including better understanding of the organization and interaction of the system in question; testing competing hypotheses about the system or process; predicting dynamics responses to internal or external stimuli; contributing to the understanding and treatment of diseases; and the personalization of medical treatments [8].

Classical pharmacology models involve model parameters that are mathematically relevant but do not generally have any physiological meaning. To be of use, these parameters must be transformed into more helpful PD/PK terms [9]. Currently, physiology is playing a larger role in the creation of these pharmacological models, and with that, the field of physiology-based pharmacokinetics (PBPK) is becoming an increasingly popular method to elucidate information on drug behavior.

1.2.2 Physiology-Based Pharmacokinetics

PBPK models are mathematically similar to traditional PK/PD models but are parametrized using known physiology to allow for a whole-body pharmacokinetic model. These models were first used by Kenneth Bischoff and Robert Dedrick in the 1960's and '70s to simulate the distribution of methotrexate, a chemotherapy drug for use in leukemia treatment [8, 10]. PBPK models behave as a hybridization of compartmental models and tank and flow systems used in chemical engineering for continuous processed. Organs or tissue areas are generally represented as boxes connected by arrows which act as blood circulatory or lymphatic influxes and effluxes to the anatomical regions. Key physiological parameters to create a model are organ volumes, volumetric flows, and physicochemical properties of the drug in questions such as tissue permeabilities, material perfusion, or binding affinity. State variables are size-based, usually concentration of the drug or material in question, so that a tissue-concentration curve can be made. Flow dynamics generally look at volumetric flow rather than mass transfer. Organs chose are those that are involved in the dynamics of the drug in question. Overall, PBPK models offer an *a priori* description of drug behavior and are useful as they can be scaled to different organisms with simple changes in the physiological parameters, which have been obtained for various species such as mice, rats, dogs, and humans [8].

1.3 Thesis Outline

In chapter 2, methods for creating a physiology-based pharmacokinetics (PBPK) model for the three QD treatments are explained. The three treatments include control quantum dots (ConQDs), calcitriol-bound quantum dots (CalQDs), and MUC1-targeting calcitriol-bound quantum dots (SM3 CalQDs). Additionally, for each

QD treatment, a simulation is run for a non-tumor mouse, a tumor-bearing mouse, and a mouse with an enlarged spleen, as is frequently seen in cancerous mice. Information is given on the organ selection, model connectivity, parameterization, and assumptions. A system of differential equations is created to describe the distribution of QD treatments.

In chapter 3, the results are given for the PBPK simulation. The partition coefficients found through the simulation are compared for all three QD treatments as well as for the different tumor or non-tumor conditions. Additionally, time course concentration data is looked at for the targeted SM3 CalQDs in each of the tumor or non-tumor conditions

In chapter 4, the results are discussed in the scope of biological relevance. The trends seen in the changes in partition coefficient as well as the trends associated with the time course concentration data are discussed in chapter 4. The results found from the PBPK simulation are compared to those previously found experimentally and potential sources of error and uncertainty are given to explain any divergence from the experimentally-discovered conclusions. Lastly, some potential future directions for this project are given.

Chapter 2

METHODS

2.1 Building the Model

2.1.1 Overall Goal

Here we will be creating a top-down model for the distribution of calcitriol quantum dots in mice for use in inflammatory breast cancer treatment. This model is based on *a priori* physical laws and parameters. After its creation and simulation using a computer program, results will be compared to experimental work down by Schaefer *et al*. on the distribution of CalQDs in mice, hence the selection of mice as the organism of interest for this model [4, 7].

2.1.2 Organ Selection

The first step to create a PBPK model is to determine the necessary organs for the model. Generally, a minimalist approach is used where the organs the specifically affect or are affected by the substance *X* are included in the model and the rest are excluded or lumped into an "other" compartment. In this case, the organs included are those relevant to calcitriol quantum dot distribution. First, the plasma compartment behaves as the central compartment by which the CalQDs are carried to and from the other tissues. Additionally, in this case we will be looking at an intravenous injection, so the substance is directly inserted into the plasma compartment as system input. The

liver is included as it is vital for clearance and breakdown of the CalQDs in the body via biliary secretion [11, 12]. The lungs and kidneys are included as they are richly perfused organs meaning they receive a significant amount of blood flow compared to other organs and tissues [8]. Additionally, previous studies have shown that QDs injected intravenously in mice localize in the liver, kidney, and spleen [4]. A single tumor compartment is also included to better understand the affinity of the targeted CalQDs to tumors. Lastly, the "other" compartment was included as a lumped compartment for tissues not explicitly mentioned. In addition to their biological involvement, experimental data exists for the concentration of CalQDs in these tissue regions allowing for validation of the model created. These organs were connected according to their physiological connection in the human body and can be seen in Figure 1.

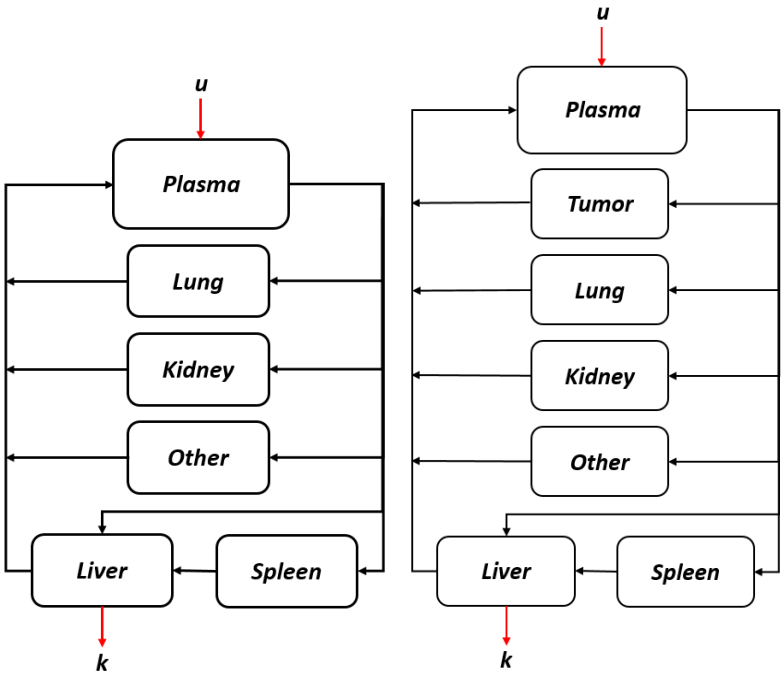

Figure 1. Connectivity for healthy, non-tumor case (left) and cancerous case (right).

2.1.3 Assumptions

The two main assumptions for this model are well-mixed and perfusion-limited approximations.

The well-mixed assumption states that each organ or tissue region is homogeneous, exhibiting no concentration gradients. This assumption is similar to that of a well-mixed tank or continuously-stirred tank used in chemical engineering. The stirring taking place inside the tank is said to be so effective that the influx concentration instantaneously reaches the concentration in the tank which is also the concentration in the efflux resulting in a uniform concentration throughout the system. This is a valid assumption for small volume tanks or compartments with low viscous

fluids. Relative to large reactor systems, mouse or even human organs are small enough that this becomes a valid assumption. Additionally, most organs' interstitial spaces are composed primarily of water, which has a relatively low viscosity. As a result, it is safe to say substances such as CalQDs are well-mixed.

The perfusion-limited (or flow-limited) assumption states that diffusion is limited by flow rate. In the case of a PBPK model, it specifically means that diffusion is limited by regional blood flow into the capillaries of an organ. A corollary from this is that tissue membranes offer no significant resistance to molecular flow relative to the blood flow. This means that diffusion across any membranes is very fast compared to blood transport. The perfusion-limited assumption is akin to the quasi-steady state approximation used in chemical engineering kinetics. This is a valid assumption based on the small size of CalQDs and lack of interactions with the tissue membranes [4].

2.1.4 Parameters Selection

The main parameters of interest to construct this PBPK model are the physiological parameters of our organism of interest, the biophysical behavior of our substance of interest, and the interactions between the two in the form of partition coefficients.

2.1.4.1 Physiological Parameters

First, we want to find the organ volumes and blood flow rate to and out of each of these organs or tissue regions. Organ masses are significantly easier to measure and can be found in literature for a multitude of organs and organisms as a fraction of body

weight [13]. Schaefer *et al*. used female mice between the ages of 13-16 weeks [7]. At this age, a typical female mouse has a mass of approximately 22.0 g [14, 15]. Knowing the body weight (BW) of the mouse, organ masses can be determined used the mean percent BW of each organ. From organ masses, organ volumes can be determined once the specific gravity of each organ is known. For the majority of organs or tissue regions, a specific gravity of 1.0 can be assumed as they are generally in this range (1.02-1.06) because they are composed primarily of water [8, 12]. There are a few notable exceptions. First, marrow-free bone has a specific gravity of 1.92 g/cm^3. Additionally, adipose volume in mice is 0.916 cm^3/100 g BW. To determine the mass of adipose in a mouse, the following equation can be use [13]:

$$(\%\, BW) = 0.0199(BW) + 1.664 \quad (1)$$

where BW is in grams. Excluding the adipose and bone, the rest of the "other" compartment volume was determined using a specific gravity of 1.0. These three were then added for the lumped "other" compartment. Utilizing these conversions, the following values for organ volumes of a healthy 22.0 g mouse were used:

Table 1. PBPK organ volumes

Tissue	**Mean % BW**	**Volume (mL)**
Kidneys	1.67	0.3674
Liver	5.49	1.2078
Lungs	0.73	0.1606
Spleen	0.35	0.077
Blood	4.9	1.078

Adipose	*2.1018*	*20.152*
Bone	*10.73*	*20.6016*
Rest	*68.1982*	*15.0036*
Other	86.86	55.7572
Tumor	--	0.08

For a 22.0 g mouse with a tumor, we used the tumor measurement given by Schaefer *et al* and added that to our organ volumes while maintaining a constant volume for the other organs [4].

The blood flow rate to each tissue region is again given as a fraction of total cardiac output. The total cardiac output for our 22.0 g female mouse can be determined from the following equation [13]:

$$Cardiac\ Output\ (L/min)\ = 0.275(BW)^{0.75} \quad (2)$$

where BW is in kg. From the mean percent cardiac outputs, blood flow to each organ can easily be determined. Additionally, the flow rate to the tumor is based on previously measured tumor blood flow rate scaled to our tumor size [16].

Table 2. PBPK organ Volumetric Flow

Tissue	**Mean % Cardiac Output**	**Flow Rate (mL/hr)**
Kidney	9.1	85.7714
Liver (Hepatic Artery)	2.0	18.8509
Liver (Portal Vein)	14.1	132.8985
Lungs	0.5	4.7127

Other	74.3	700.3091
Tumor	--	1.7664

2.1.4.2 Biophysical Parameters

CalQDs are injected intravenously into the organism, so input is modeled as a pulse into the plasma compartment. Effectively, this behaves as the plasma compartment starting with an initial concentration equal to that of the IV injection and distributing to the rest of the body as time progresses.

The sink for CalQDs is from the liver compartment in the form of biliary excretion which takes the form of a first-order kinetic degradation of concentration with time. The following estimation for the first-order clearance rate constant was previously validated from experimental data for QD 705 [11]. The value is very small because QD clearance from the body is slow with significant concentrations still measured even 28 days after intravenous injection.

$$k_{elim} = 1.0 \times 10^{-6}\ hr^{-1} \quad (3)$$

Because the system is assumed to be perfusion-limited, membrane permeabilities and transport mechanisms can be neglected at this stage. Additionally, CalQDs are assumed to be free moving molecules, so binding affinities are also unnecessary.

2.1.4.3 Partition Coefficients

A partition coefficient, *P*, is the equilibrium tissue-to-blood partition coefficient which is a proportionality constant relating the tissue concentration of

substance *X* to the outgoing venous concentration. In the perfusion-limited case, *P* describes the ratio of the total tissue concentration of a substance *X* to its concentration in the outgoing blood flow. In practice, *P* is approximated by the empirical equilibrium partition coefficient, which effectively lumps all process that alter tissue extraction together in one term and is estimated experimentally using *in vitro* experimentation. It is then extrapolated to the whole organ assuming uniform concentration throughout the tissue [8].

Due to the novelty of targeted CalQDs, experimental partition coefficients do not yet exist, so estimation will be used going forward based on the concentrations measured by Schaefer *et al* [7]. It is recommended going forward that more *in vitro* experimentation is done on SM3 CalQDs, so that a full *a priori* model can be created using existing biochemical behavior of the molecules instead of estimation techniques. The main point of this study is to create a model backbone for the physical behavior and distribution of CalQDs and targeted CalQDs in mice. Future experimentation can be then used to augment this model with more biologically accurate partition coefficients.

For untargeted CalQDs, some partition coefficients are available for QD 705 [11]. Assuming that calcitriol conjugated to QDs does not significantly affect the distribution of QDs in tissue, we can use these values as a starting point.

Table 3. Initial Estimates for Organ Partition Coefficients

Tissue	**Partition Coefficient (P)**
Kidneys	7.42

Liver	10.9
Spleen	33.35
Lungs	2.37
Lumped tissue	5.0

2.1.5 Single Organ Equation

The equations for the organs are mass flow balances across homogeneous, well-stirred tissues with influx and efflux. For a constant volume, mass flow (mass/time) is equivalent to the constant volume (vol) multiplied by concentration (mass/vol). The substance *X* is said to flow at the same rate into the organ as out of the organ with the change being in the concentration of the substance in the inflow (arterial concentration) compared to the outflow (venous concentration) due to distribution into the tissue. Additionally, an organ may have a sink or source, which will be represented here as a rate, *R*. Overall, this gives the following equation for a single organ system (Eqtns. 4-8).

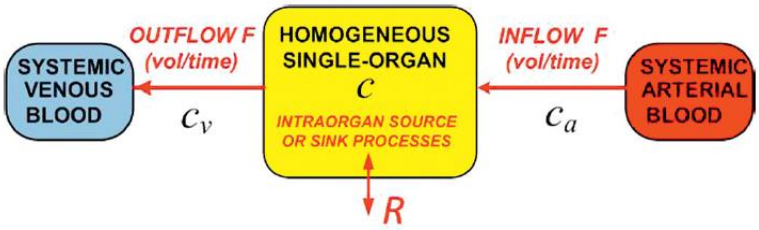

Figure 2. Single organ PBPK model [8].

$$[mass\ flow\ rate] = [rate\ of\ mass\ in] - [rate\ of\ mass\ out] + [rate\ of\ mass\ generated\ or\ lost\ from\ source\ or\ sink] \quad (4)$$

$$[mass\ flow\ rate] = [rate\ of\ volumetric\ flow]([concentration\ of\ substance\ X\ entering] - [concentration\ of\ substance\ X\ exiting] + [rate\ of\ mass\ generated\ or\ lost\ from\ source\ or\ sink]) \quad (5)$$

$$\dot{Q} = V\dot{c} = F(c_i - c_o) + R \quad (6)$$

Because we are interested in the concentration in the actual tissue rather than in the circulatory system, we will utilize the partition coefficient, *P*, which again is the ratio of concentration of substance *X* in the tissue to the venous concentration of substance *X*.

$$P = \frac{c}{c_o} \quad (7)$$

Substituting this into the equation, we have the following equation to describe a single organ system:

$$\dot{Q} = V\dot{c} = F\left(c_i - {}^{c}/_{P}\right) + R \quad (8)$$

2.1.6 Multiple Organ System

Thus, for our healthy, non-tumor system containing the kidneys, liver, lungs, spleen, and plasma, with pulse input and excretion from the liver following first-order kinetics, we have the following set of differential equations:

$$\dot{C}_{blood(b)} = \left(\frac{1}{V_b}\right)\left\{\left[\left(\frac{Q_k C_k}{P_k}\right) + (Q_{li} + Q_s)\frac{C_{li}}{P_{li}} + \left(\frac{Q_l C_l}{P_l}\right) + \left(\frac{Q_o C_o}{P_o}\right)\right] - (Q_{total})C_b\right\} \quad (8)$$

$$Q_{total} = Q_{kidney} + Q_{liver} + Q_{spleen} + Q_{lung} + Q_{other} \quad (9)$$

$$\dot{C}_{kidney(k)} = \left(\frac{Q_k}{V_k}\right)\left[C_b - \frac{C_k}{P_k}\right] \quad (10)$$

$$\dot{C}_{lung(l)} = \left(\frac{Q_l}{V_l}\right)\left[C_b - \frac{C_l}{P_l}\right] \quad (11)$$

$$\dot{C}_{spleen(s)} = \left(\frac{Q_s}{V_s}\right)\left[C_b - \frac{C_s}{P_s}\right] \quad (12)$$

$$\dot{C}_{liver(li)} = \left(\frac{1}{V_{li}}\right)\left[Q_{li}C_b + Q_s\frac{C_s}{P_s} - (Q_{li} + Q_s)\frac{C_{li}}{P_{li}} - kC_{li}\right] \quad (13)$$

$$\dot{C}_{other(o)} = \left(\frac{Q_o}{V_o}\right)\left[C_b - \frac{C_o}{P_o}\right] \quad (14)$$

For the unhealthy case including a tumor, the blood compartment and overall mass flow as well as the addition of a tumor equation. The rest of the equations remain the same. The new differential equations are as follows:

$$\dot{C}_{blood(b)} = \left(\frac{1}{V_b}\right)\left\{\left[\left(\frac{Q_k C_k}{P_k}\right) + (Q_{li} + Q_s)\frac{C_{li}}{P_{li}} + \left(\frac{Q_l C_l}{P_l}\right) + \left(\frac{Q_o C_o}{P_o}\right) + \left(\frac{Q_t C_t}{P_t}\right)\right] - (Q_{total})C_b\right\} \quad (15)$$

$$Q_{total} = Q_{kidney} + Q_{liver} + Q_{spleen} + Q_{lung} + Q_{other} + Q_{tumor} \quad (16)$$

$$\dot{C}_{tumor(t)} = \left(\frac{Q_t}{V_t}\right)\left[C_p - \frac{C_t}{P}\right] \quad (17)$$

2.2 Solving the Equations

Equations were solved simultaneously using the built-in function ode23s on MATLAB® R2017a. All above parameters were used except for the partition

coefficients which were varied from their original estimations under the model output could be validated by experimental data. Validation was done with concentration data for kidneys, spleen, liver, and lungs for a mouse with and without a tumor taken at day 4 after intravenous injection in mice with ConQDs, CalQDs, or SM3 CalQDs by Schaefer *et al* [4, 7].

To understand the whole organism behavior of QDs in the unhealthy, tumor case, estimations were made for the concentration of QDs in the tumor based on expected behavior. In the tumor case, for the ConQDs and untargeted CalQDs, we would expect concentrations of the QDs in the tumor to be similar to the other organs, while for targeted QDs, we would expect the concentrations of QDs to be significantly higher in the tumor than in the other tissue regions. To begin, we will set the concentration for both ConQDs and CalQDs to the average value of QD concentrations in the other organs. This works to elucidate information on the behavior of the partition coefficients in the other organs in response to a tumor. In the case of SM3 targeted CalQDs, the concentration of QDs in the tumor compartment ideally be the highest. The model this behavior, we will look at a concentration in the tumor as slightly higher than the maximum concentration observed in any of the organs as these QDs are specifically designed to target tumor cells.

Table 4. Estimation of Concentrations of Various QDs in the Tumor Compartment

Tissue	**ConQD Concentration**	**CalQD Concentration**	**SM3 CalQD Concentration**
Tumor	15.51	16.0875	30

In addition, we will look at the effects of an increase in volume of the spleen on the organ partition coefficients, as an increase in spleen size can frequently be seen in cancer patients due to abnormal white cells that invade the spleen. The volume of the spleen can reach up to twice its usual volume as a result [18]. While we will look at an increased spleen volume, we will maintain the spleen blood flow rates as the only way to increase flow is to add new blood vessels which takes weeks. At the time scale of 4 days, this is not relevant.

Chapter 3

RESULTS

Partition coefficients for ConQDs, CalQDs, SM3 CalQDs across all tissue regions in the non-tumor, tumor, and enlarged spleen cases can be seen below. Tables of values found can be seen in Appendix B.

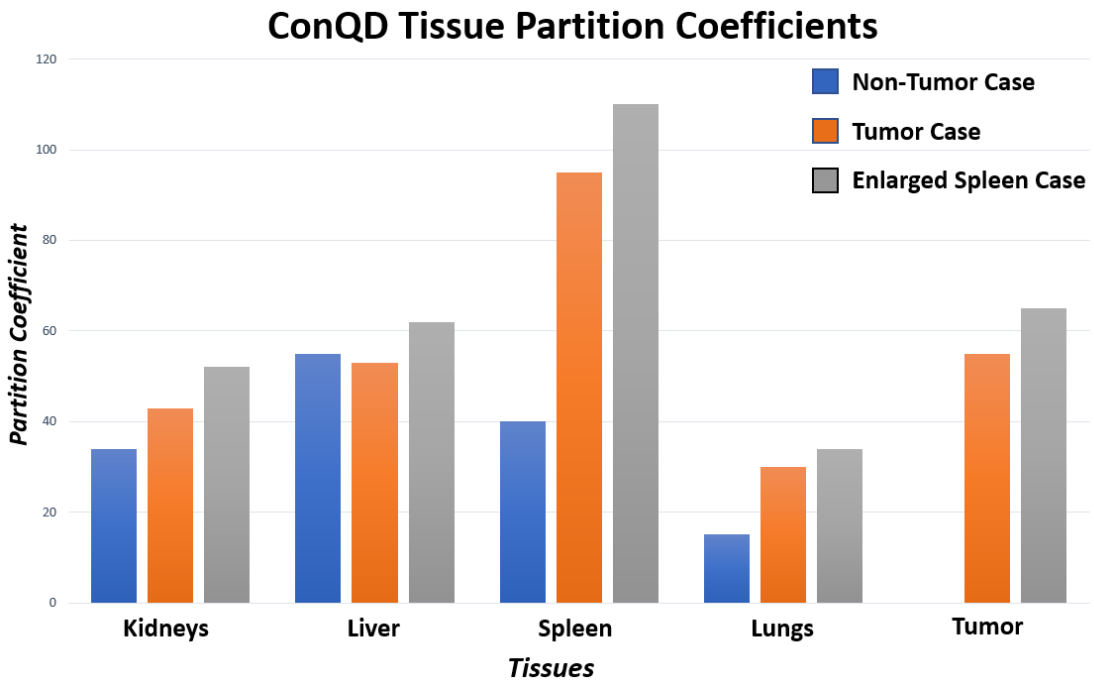

Figure 3. Tissue partition coefficients for ConQDs in all tissue regions for the non-tumor, tumor, and enlarged spleen cases.

Overall, the tissue partition coefficients tend to increase from the non-tumor to tumor case and again with the enlarged spleen. The kidneys exhibit approximately the same increase in partition coefficient between all three cases. It also exhibits the second lowest partition coefficients. The liver does not follow the increase in partition coefficients seen in the other tissues and, instead, remains approximately constant and consistently high across all cases. The spleen is initially lower than the kidney, but with the introduction of a tumor, its *P* significantly increases. The lungs consistently have the smallest *P* in all cases. Lastly, the tumor values are high but still lower than the spleen.

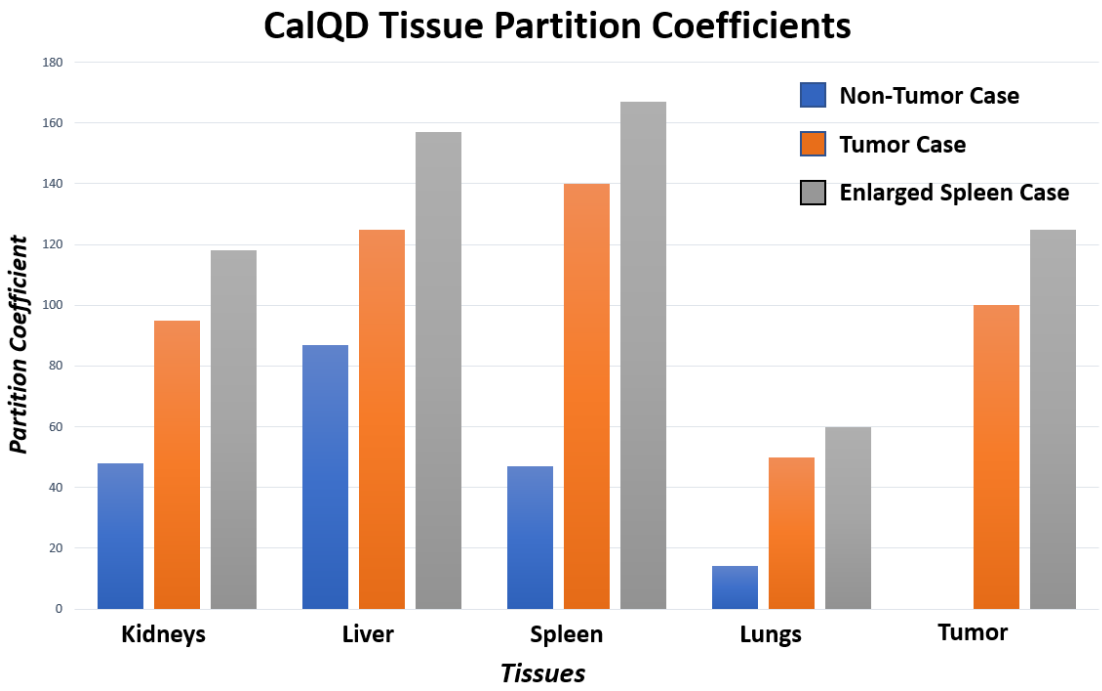

Figure 4. Tissue partition coefficients for CalQDs in all tissue regions for the non-tumor, tumor, and enlarged spleen cases.

In the CalQD case, the partition coefficients are consistently higher than in the ConQD case. Similar to the ConQD case, there is a general increase in partition coefficients from the non-tumor to the tumor case and again to the enlarged spleen. Unlike the ConQD case, the liver is not approximately constant and does exhibit an increase similar to other organs. Again, the spleen *P* significantly increases with the introduction of a tumor. The lungs also still have the lowest *P* values. Tumor values are high but lower than the liver as well as the spleen in this case.

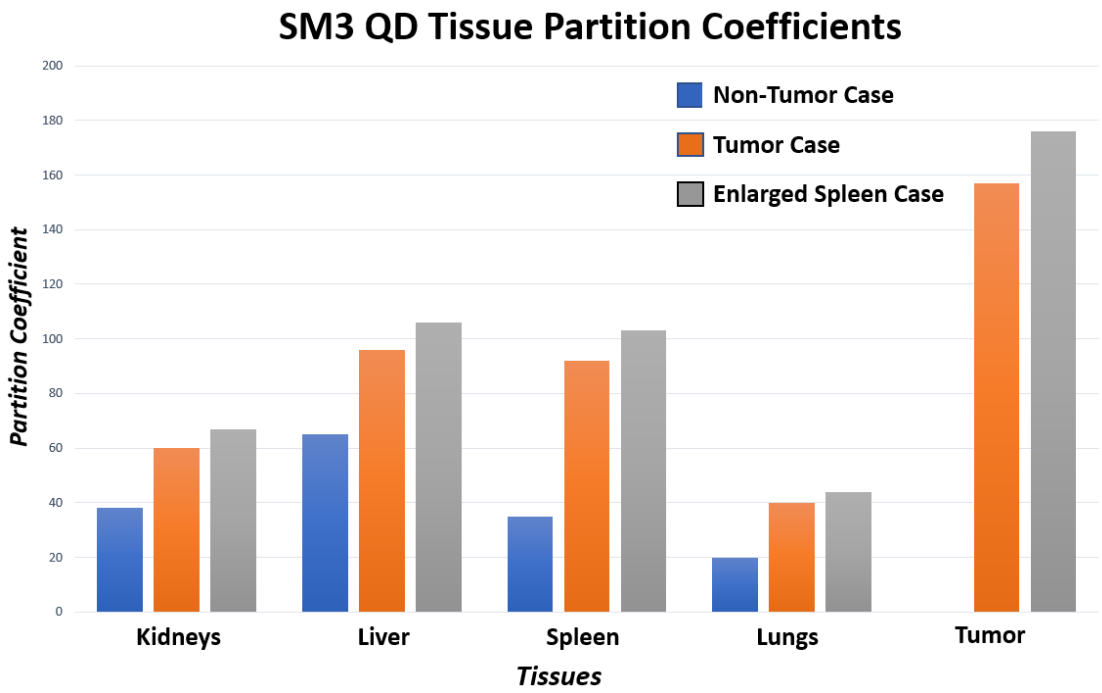

Figure 5. Tissue partition coefficients for SM3 CalQDs in all tissue regions for the non-tumor, tumor, and enlarged spleen cases.

In the SM3 CalQD case, partition coefficients are lower than in the CalQD case except for the tumor tissue. Again, we see an increase in *P* across all tissues from the non-tissue to tissue to enlarged spleen, but the increase is not as extreme as in the case of ConQDs. Similar to the other two cases, we see a significant increase in partition coefficient in the spleen once a tumor is introduced, and the lungs still have the lower *P*.

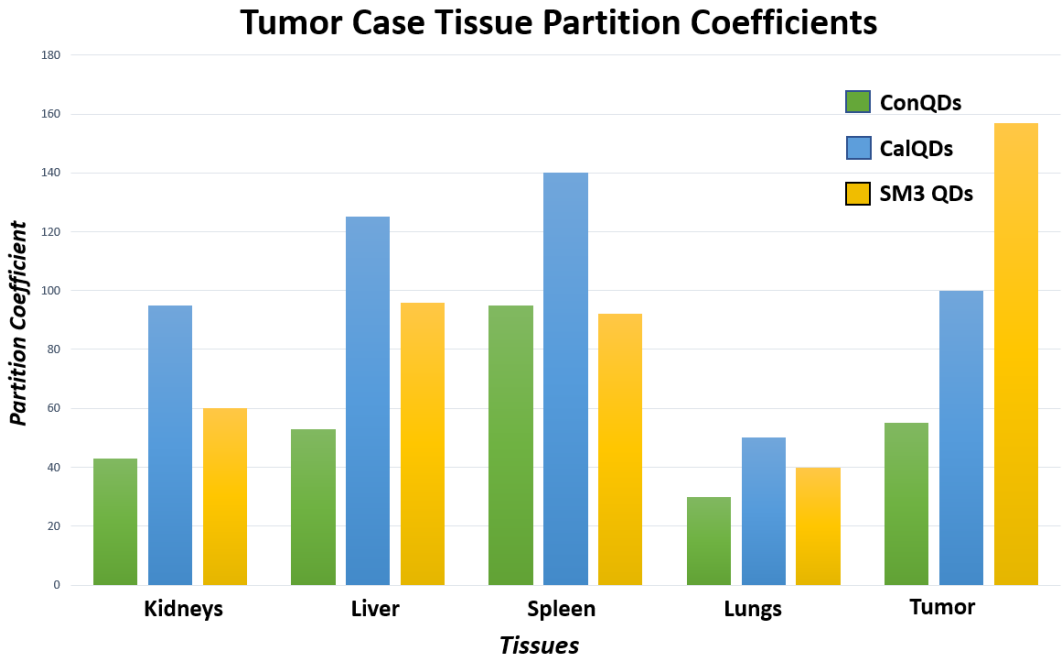

Figure 6. Tissue partition coefficients for tumor condition in all tissue regions for ConQDs, CalQDs, and targeted SM3 CalQDs.

CalQDs have the highest partition coefficient in all tissues except the tumor tissue, which has the highest partition coefficient in the SM3 CalQD case. Consistently, lungs have the lowest *P* values. Spleen generally has the highest *P* of all

organs except it is slightly lower than the partition coefficient of SM3 CalQDs for the liver tissue. Additionally, the SM3 CalQD partition coefficient is higher than the ConQD *P* for all tissues except the spleen where it is slightly lower.

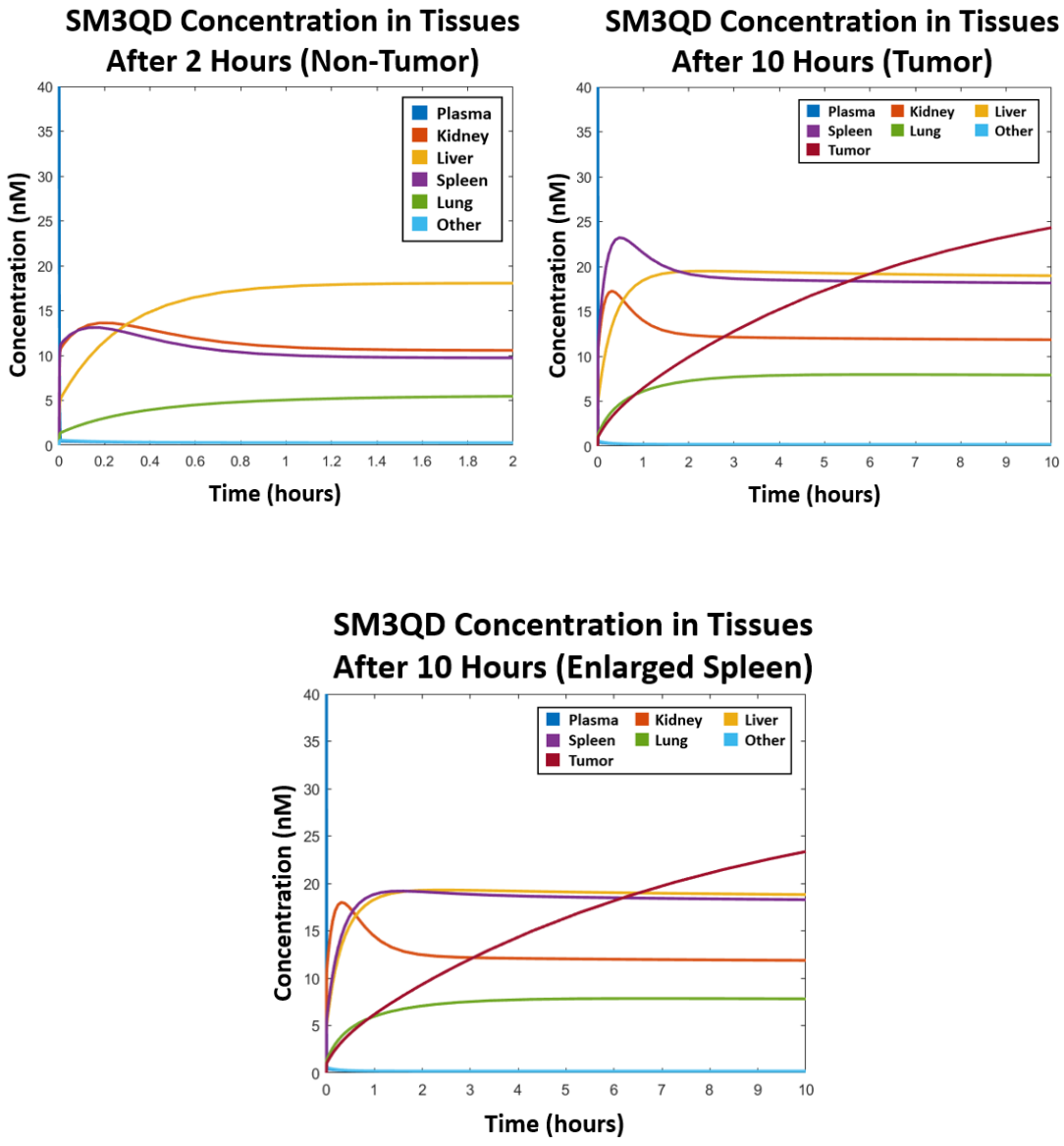

Figure 7. Tissue concentration-time data for SM3 CalQDs in the non-tumor, tumor, and enlarged spleen cases.

Time-concentration data for SM3 CalQD distribution can be seen in Figure 7. The time-concentration data for all other cases can be found in Appendix C. The QD concentration decreases from 40 nM in the plasma as it is redistributed to other tissue regions and eventually excreted from the liver. In the case of ConQDs and CalQDs, the QD concentration peaks and decreases in the kidney and spleen as it redistributes into other tissues. For the SM3 CalQDs, the peak is only seen for the kidney tissue, not the spleen. The other tissue regions exhibit an increase over the whole time range. The concentration curves being to level and constantly decrease after two hours in the case of ConQDs and ten hours for CalQDs and SM3 CalQDs.

Chapter 4

DISCUSSION

4.1 Overview

Inflammatory breast cancer is an aggressive and deadly form of breast cancer known for its highly metastatic tumor emboli. Previous studies have indicated calcitriol has an effect against the metastasis of IBC cells, but high levels of calcitriol are required to see these beneficial results. As a result, the use of calcitriol in IBC has been limited. SM3 CalQDs have exhibited tumor targeting capabilities for calcitriol treatment of IBC cells [4]. A physiology-based pharmacokinetic model provides an additional tool that can be used to augment *in vitro* and *in vivo* studies to better understand the mechanisms behind the distribution of SM3 CalQDs on a system level.

4.2 Summary of Results

Overall, we were able to demonstrate that a physiology-based pharmacokinetic model can be used to describe the behavior and distribution of QDs both in non-tumor and tumorous mice. While at this point we do not have *a priori* partition coefficient data for any of the QDs in question, we are still able to look at the effects of different partition coefficients in giving simulated data consistent with that found experimentally. Additionally, we are able to highlight the differences in partition coefficients between ConQDs, CalQDs, and SM3 QDs as well as non-tumor and tumor cases. We also observed changes in partition coefficients with changes in spleen

volume that would be expected in cancer patients. Lastly, we are able to use our model to look at time-concentration data of QDs in several tissue regions.

4.3 Discussion of Changes in Partition Coefficient

The changes in partition coefficient values provide interesting insight into the dynamics of the system at hand. As previously mentioned, the partition coefficient describes the ratio of the concentration of a substance *X* (in this case the QDs) in the tissue to the concentration of substance *X* in the efflux venous flow. We can understand an increase in partition coefficient being an increase in QD entering the tissue from the capillaries under a given condition. Thus, given the previously found concentrations of QDs observed in various tissue regions, we see a general increase in uptake of QDs in all regions when a patient has IBC [4]. The opposite of this is also true indicating that healthy patients have a decrease flow of QDs into the tissues.

It has been previously reported that calcitriol is able to mitigate negative effects of tumors, so the best condition for a patient with IBC is where the tumor tissue exhibits a high partition coefficient, representing more calcitriol accumulating in the tumor [4]. With this in mind, the targeted SM3 QDs provides the largest amount of calcitriol to the tumor area of interest for this model. The concern here would be that the tumor concentrations were estimated and are not known for sure, so it is recommended that further testing be done to validate this hypothesis. In the case of SM3QDs in a tumor patient, the liver and spleen also exhibit relatively high uptake of QDs.

4.4 Discussion of Time-Concentration Data

Another important feature of this model is its ability to highlight the QD distribution at multiple time points in different tissue regions. Given that IBC is highly metastatic, this is valuable information as tumor emboli could metastasize to these tissue regions. Therefore, this model is able to demonstrate which areas currently have a high level of QD uptake due to their high partition coefficients. This information is also important to avoid potential hypercalcemia in patients undergoing treatment.

This model is able to predict concentration data over a continuous time range, which has not previously been done. As a result, we are able to observe and compare the differences in short-term and long-term behavior of various QDs in each tissue region. Looking more in-depth at the behavior of SM3QDs in the body, we can see for IBC patients a spike and subsequent drop-off of concentration levels in the spleen and kidney as the QDs redistribute to other tissue regions. For this simulation, the spike observed does not exceed the initial dosage, so concerns around hypercalcemia are not relevant here, but further simulations for other conditions could be used to verify safe levels of calcitriol are maintained. With an increase in spleen volume, we observe an interesting change in the initial behavior of SM3QDs in the spleen. Instead of a spike and decrease, there is behavior more similar to the uptake in the liver.

4.5 Comparison to Literature

Similar to the experiment done by Schaefer *et al*, SM3 CalQDs were also seen to be taken up in the tumor more than CalQDs, but they were not consistently retained longer than other treatments. The concentration profiles after 3 days suggest some higher concentrations in tissues for SM3 CalQDs compared to other treatments and

some lower values, which is not consistent with the findings of Schaefer *et al*. Additionally, the maximum concentrations were seen to be within the first day while Schaefer found the maximum concentrations to be at Day 2 rather than Day 1. Despite the treatment, QDs were present in the tumor. This is thought to be a result of the leaky vasculature of tumors [4, 7].

QD concentration in the lungs is of interest as the lungs are the most common site for IBC tumor metastasis. Consistent with Schaefer's finding, all QD treatments exhibited a higher concentration of QDs in the lung tissue for tumor-bearing mice compared to healthy mice. Additionally, all treatments have similar amounts of QD accumulating in the lungs [4, 7].

4.6 Causes of Error and Uncertainty

For this study, partition coefficients were determined using QD concentrations observed in tissue regions after 4 days. Generally, PBPK models use a priori data to build a top-down model of the system in question. With that being said, empirical equilibrium partition coefficients obtained from in vitro studies are used to predict concentration-time data for various tissue regions. Thus, to build a fully top-down model, we hope to run further in vitro and in vivo studies on the uptake of CalQDs and SM3QDs in tissue cells. From that, we would be able to confidently predict the concentration data for each region without the estimations made in this work.

4.7 Future Directions

There are multiple future directions for this project. One would be to separate each compartment into a tumor and non-tumor compartment instead of a single tumor compartment and compare the results of a model connected like this. This would be useful as IBC is known to be highly metastatic, meaning the tumor emboli distribute and accumulate in other parts of the body in addition to the breast.

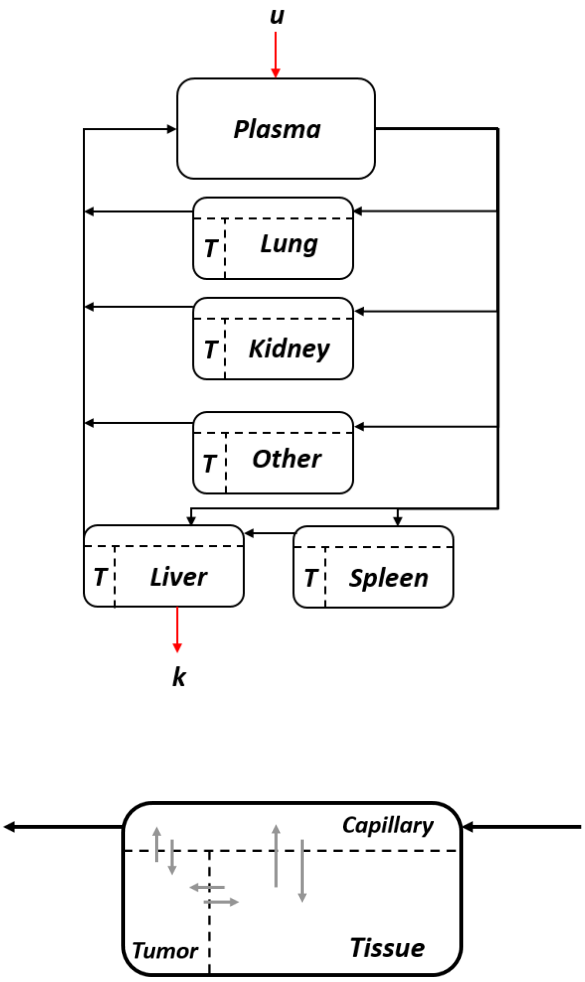

Figure 8. (top) Multi-tumor compartment model connectivity across the whole body and (bottom) distribution between the capillary, tissue, and tumor.

Another direction would be to include a unique adipose tissue rather than lumping it in the "other" compartment to observe the distribution into the adipose which would be representative of the breast tissue. This would be important as breast cancer initially begins in the breast of cancer patients.

Currently, the blood circulatory system is the primary method of distribution in the scope of this model, but the lymph system could be included as well. That was, information would be elucidated about the behavior of tumor emboli metastasizing through the body via the lymphatic system.

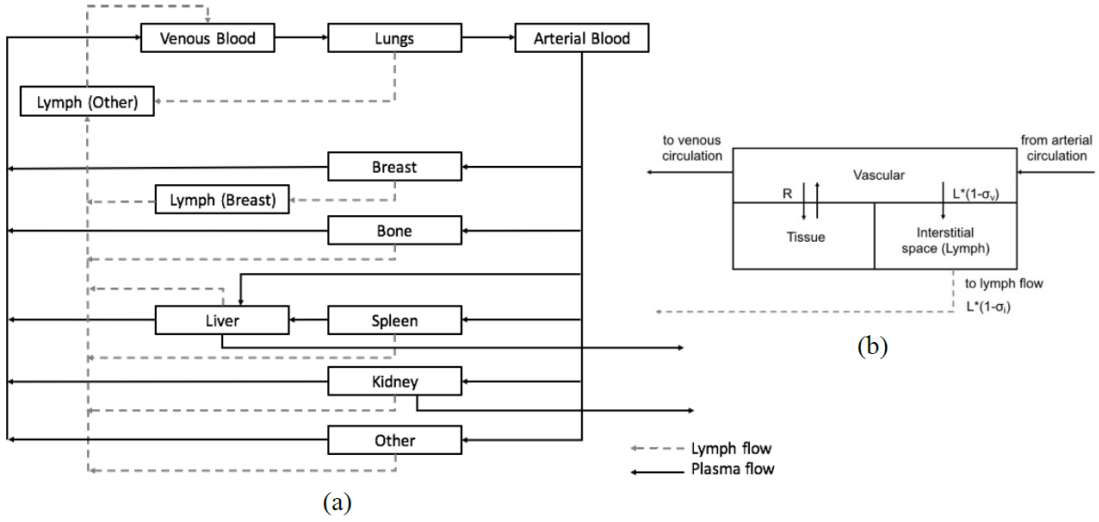

Figure 9. (a) Connectivity map of PBPK model with the addition of the lymphatic system. (b) Sub-compartment diagram including three parts: vascular, tissue, and interstitial space.

Lastly, if funding allows for it, further *in vitro* experiments should be run to determine the partition coefficients and obtain distribution data about the behavior of QD treatments to better validate the PBPK models discussed above.

4.8 Conclusion

Here we have constructed and validated a PBPK model for multiple QD treatment strategies for IBC. It is recommended that further *in vitro* analysis of the QD treatments be done so currently estimated parameters can be replaced by physiologically accurate ones to complete the top-down model. SM3 CalQDs provide a targeted calcitriol treatment for IBC cells, which is important to mitigate cancerous effects of the tumor cells will allowing for live cell direct imaging and avoiding hypercalcemia in patients. Hopefully, this model can be used to expedite research on QD treatment alternatives.

Link to MATLAB code: https://github.com/mwagner92796/senior-thesis

REFERENCES

1. Inflammatory Breast Cancer. *National Cancer Institute*, National Institute of Health (2016). https://www.cancer.gov/types/breast/ibc-fact-sheet.

2. Robertson, F. M. *et al*. Inflammatory breast cancer: the disease, the biology, the treatment. *CA. Cancer J. Clin.* **60**, 351–75 (2010).

3. Hillyer, R. L. *et al.* Differential effects of vitamin D treatment on inflammatory and non-inflammatory breast cancer cell lines. *Clin. Exp. Metastasis* **29**, 971–9 (2012).

4. Schaefer, R. J. *et al.* Targeting of Calcitriol to Inflammatory Breast Cancer Tumors and Metastasis In Vitro and In Vivo. *Biol. Syst.* **1**, 1–7 (2012).

5. Lehmann, B. *et al.* Vitamin D metabolism. *Dermatol Ther.* **23**(1): p. 2-12 (2010).

6. Beer, T. M. & Myrthue, A. Calcitriol in cancer treatment: from the lab to the clinic. *Mol. Cancer Ther.* **3**, 373–381 (2004).

7. Schaefer, R. J. Calcitriol Conjugated Quantum Dots, An Innovative Tool as Both Probe and Treatment, (2012).

8. DiStefano, J. Dynamic Systems Biology Modeling and Simulation. *Elsevier*. **1**, 2-11, 345-372 (2013).

9. Jones, H. & Rowland-Yeo, K. Basic Concepts in Physiologically Based Pharmacokinetic Modeling in Drug Discovery and Development. *CPT: Pharmacometrics & Systems Pharmacology*, **2**: 1-12 (2013).

10. Bischoff, K. B. *et al*. Methotrexate Pharmacokinetics. *J. of Pharma. Sci*. **60** (8): 1128-1132 (1971).

11. Li, M., Al-Jamal, K. T., Kostarelos, K. & Reineke, J. Physiologically Based Pharmacokinetic Modeling of Nanoparticles. *ACS Nano*. **4**, 6303–6317 (2010).

12. Lin, P. *et al*. Computational and ultrastructural toxicology of a nanoparticle, Quantum Dot 705, in mice. *Environ. Sci. Technol*. **42**, 6264–6270 (2008).

13. Brown, R. P. *et al*. Physiological Parameter Values for Physiologically Based Pharmacokinetic Models. *Toxicol. Ind. Health.* **13** (4): 407-484 (1997).

14. Body Weight Information for C57BL/6J. *The Jackson Laboratory*. (2018). https://www.jax.org/jax-mice-and-services/strain-data-sheet-pages/body-weight-chart-000664#.

15. Rat and Mice Weights. *Animal Resources Centre.* (2018). http://www.arc.wa.gov.au/?page_id=125.

16. Sakaeda T. *et al.* Blood Flow Rate in Normal and Tumor-Bearing Rats in Conscious State, under Urethane Anesthesia, and during Systemic Hypothermia. *Journal of Drug Targeting*. **6**(4): 261-272 (2009).

17. Yank, R.S.H. *et al.* Persistent Tissue Kinetics and Redistribution of Nanoparticles, Quantum Dot 705, in Mice: ICP-MS Quantitative Assessment. *Environment Health Perspectives.* **115**(9): 1339-1343 (2007).

18. Wedro, B. Enlarged Spleen (Splenomegaly) Symptoms, Signs, Causes, and Treatment. *MedicineNet, Inc.* (2018). https://www.medicinenet.com/enlarged_spleen/article.htm#can_an_enlarged_spleen_be_prevented.

Appendix A

CONCENTRATION COMPARISIONS

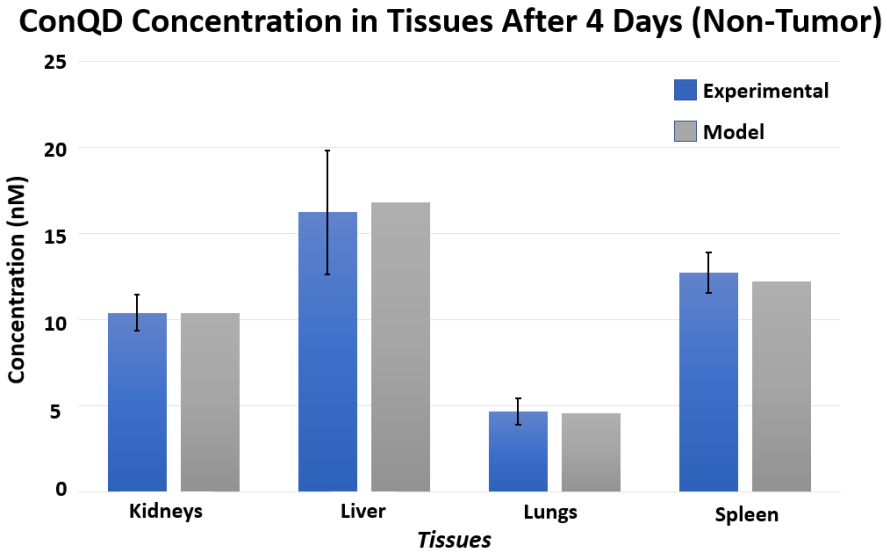

Figure 10. Comparison of concentration between experimental and model data in tissue regions for ConQD treatment in healthy, nontumor-bearing mice.

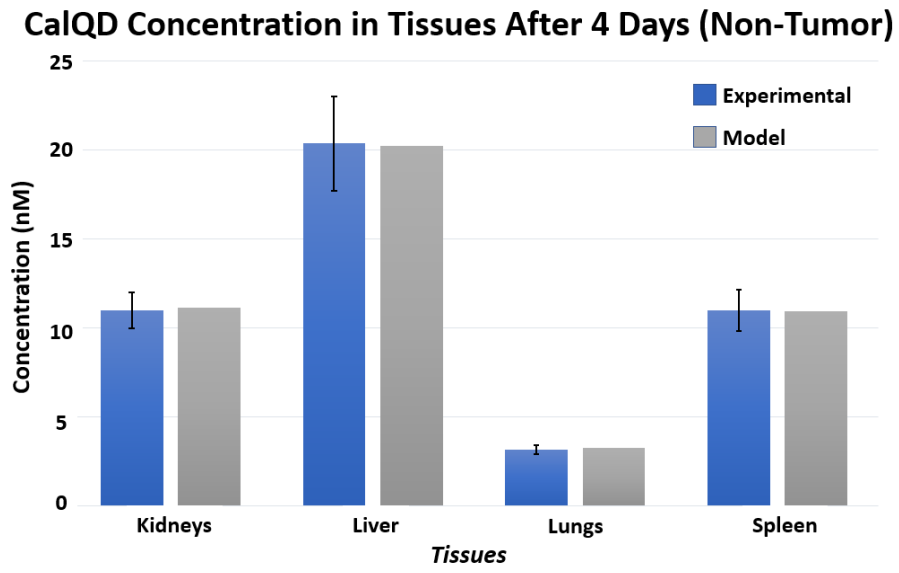

Figure 11. Comparison of concentration between experimental and model data in tissue regions for CalQD treatment in healthy, nontumor-bearing mice.

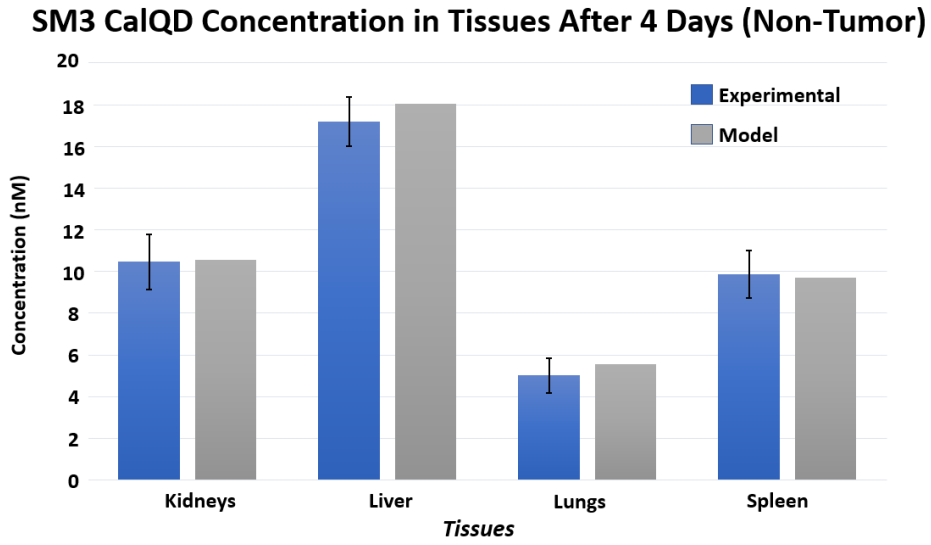

Figure 12. Comparison of concentration between experimental and model data in tissue regions for SM3 CalQD treatment in healthy, nontumor-bearing mice.

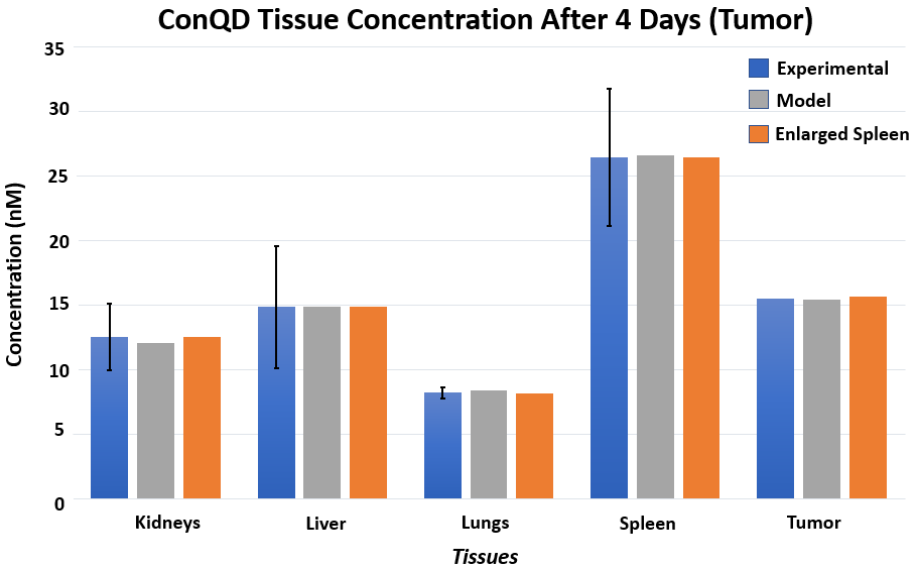

Figure 13. Comparison of tissue concentrations found experimentally (blue), using the PBPK model (grey), and for the increase in spleen volume (orange) for tumor-bearing mice using ConQDs.

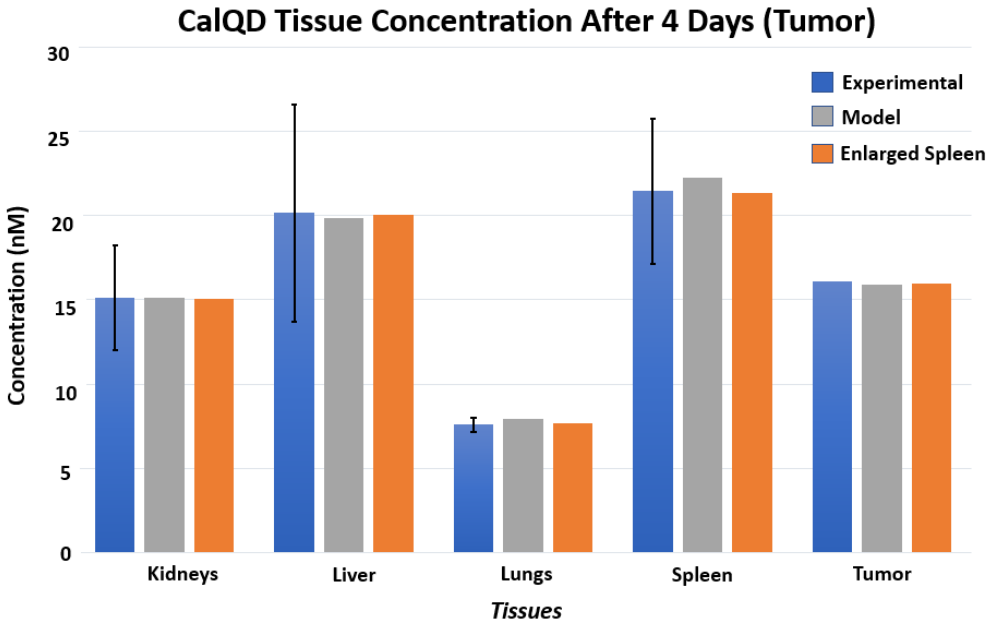

Figure 14. Comparison of tissue concentrations found experimentally (blue), using the PBPK model (grey), and for the increase in spleen volume (orange) for tumor-bearing mice using CalQDs.

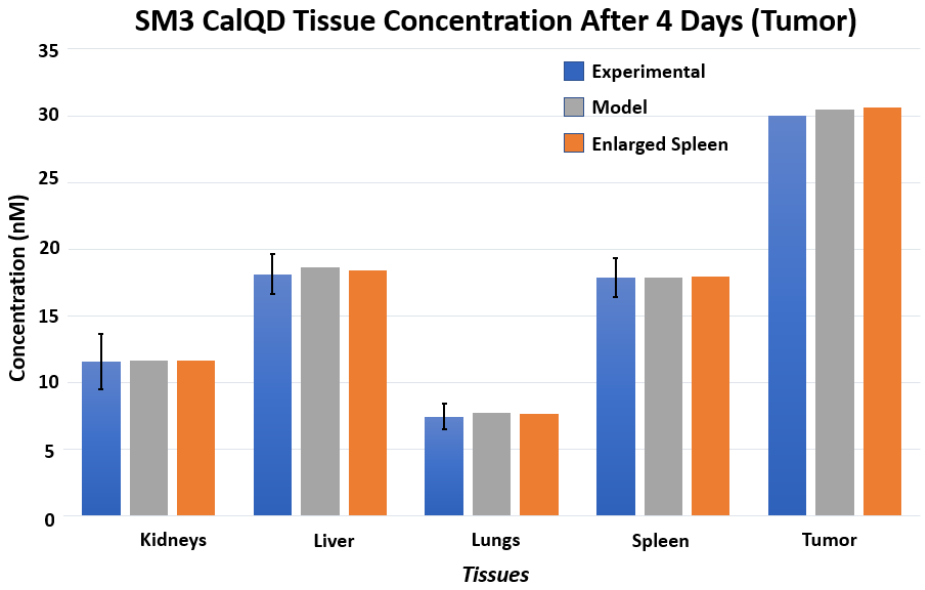

Figure 15. Comparison of tissue concentrations found experimentally (blue), using the PBPK model (grey), and for the increase in spleen volume (orange) for tumor-bearing mice using SM3 CalQDs.

Appendix B

TISSUE PARTITION COEFFICIENTS

Table 5. Nontumor-bearing mice tissue partition coefficient for each treatment.

Tissue	**ConQD *P***	**CalQD**	**SM3 CalQD**
Kidney	34	48	38
Liver	55	87	65
Spleen	40	47	35
Lungs	15	14	20

Table 6. Tumor-bearing mice tissue partition coefficient for each treatment.

Tissue	**ConQD *P***	**CalQD**	**SM3 CalQD**
Kidney	43	95	60
Liver	53	125	96
Spleen	95	140	92
Lungs	30	50	40
Tumor	55	100	157

Table 7. Tumor-bearing mice tissue partition coefficient for each treatment in the case of an enlarged spleen.

Tissue	**ConQD *P***	**CalQD**	**SM3 CalQD**
Kidney	52	118	67
Liver	62	157	106
Spleen	110	167	103
Lungs	34	60	44
Tumor	65	125	176
Avg % increase	17.0	22.8	22.1

Appendix C

TIME-CONCENTRATION GRAPHS

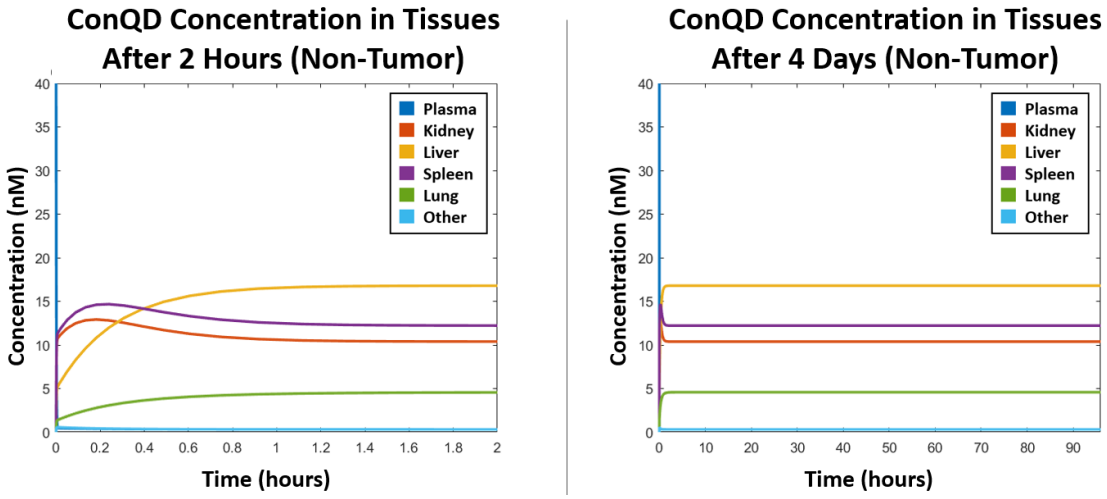

Figure 16. ConQD treatment time-concentration data for nontumor-bearing mice in each tissue region after 2 hours (left) and 4 days (right).

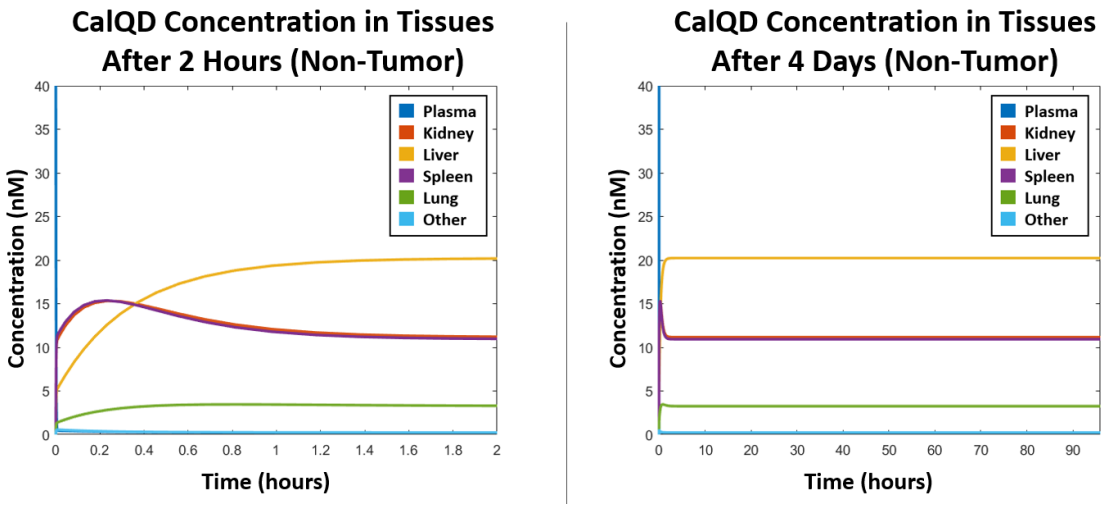

Figure 17. CalQD treatment time-concentration data for nontumor-bearing mice in each tissue region after 2 hours (left) and 4 days (right).

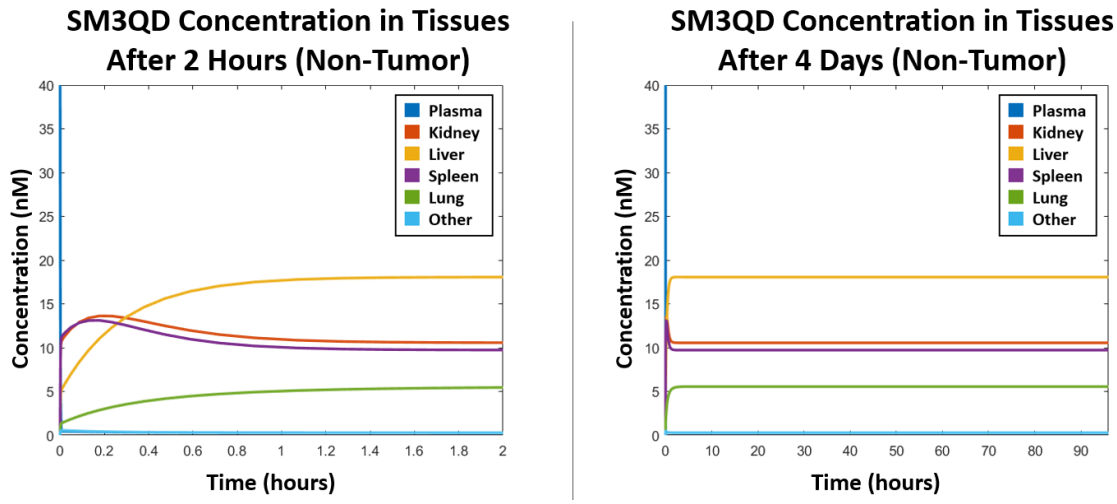

Figure 18. SM3 CalQD treatment time-concentration data for nontumor-bearing mice in each tissue region after 2 hours (left) and 4 days (right).

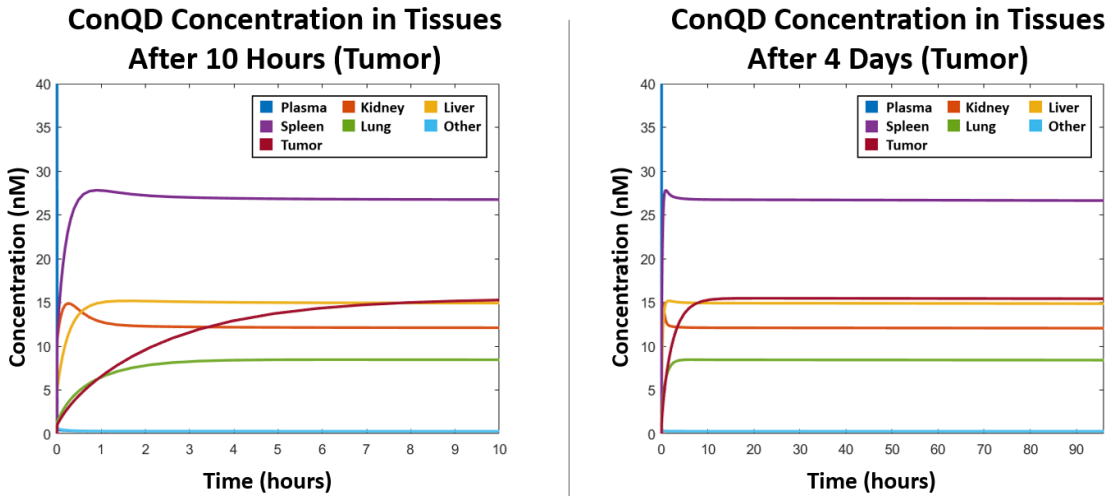

Figure 19. ConQD treatment time-concentration data for tumor-bearing mice in each tissue region after 10 hours (left) and 4 days (right).

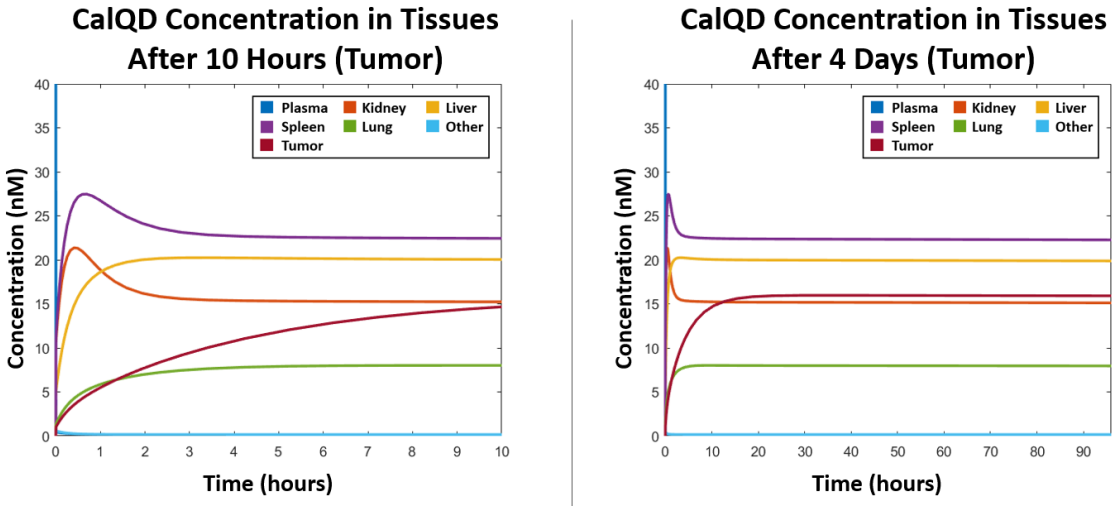

Figure 20. CalQD treatment time-concentration data for tumor-bearing mice in each tissue region after 10 hours (left) and 4 days (right).

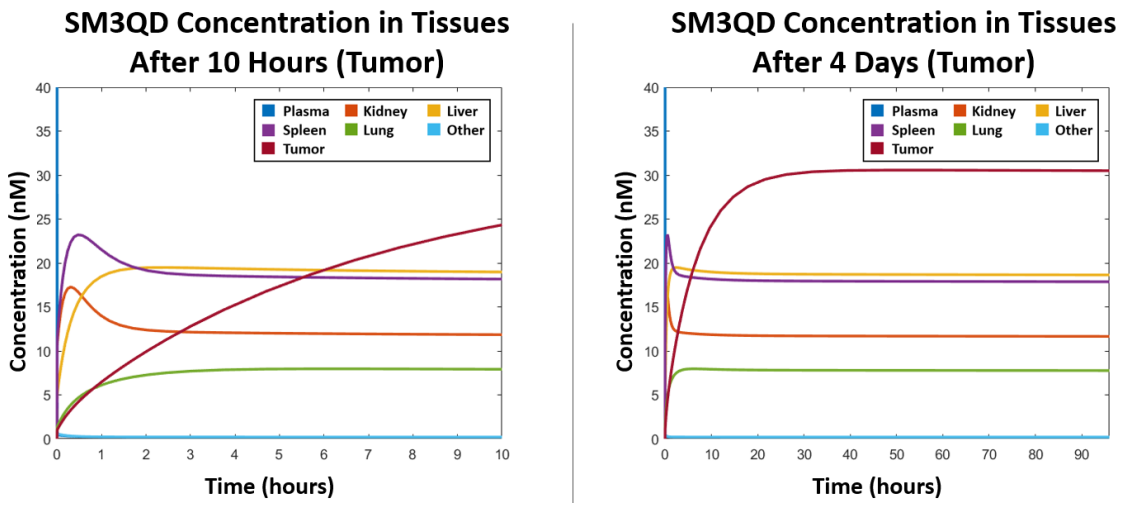

Figure 21. SM3 CalQD treatment time-concentration data for tumor-bearing mice in each tissue region after 10 hours (left) and 4 days (right).

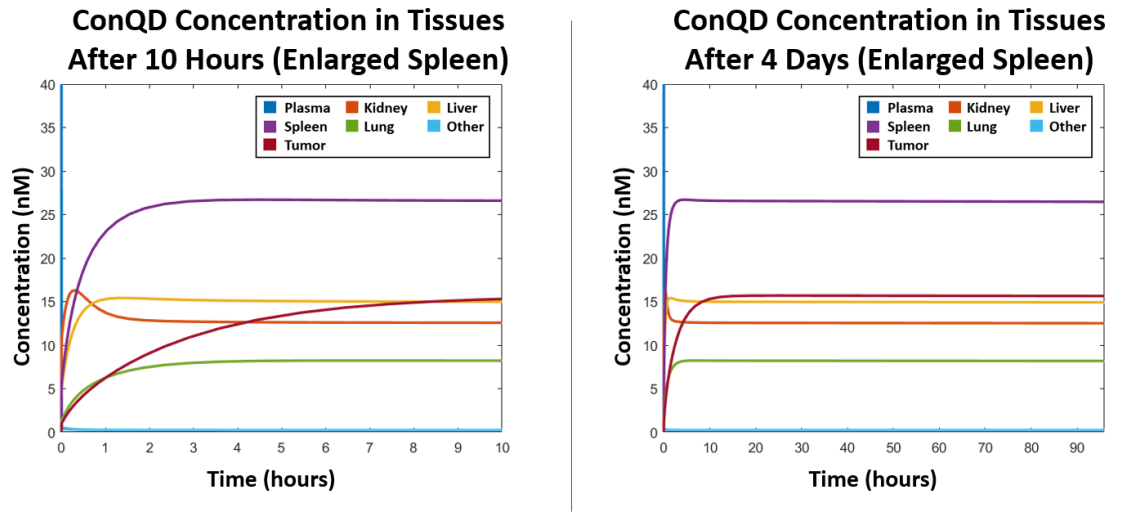

Figure 22. ConQD treatment time-concentration data for tumor-bearing mice in each tissue region in the case on an enlarged spleen after 10 hours (left) and 4 days (right).

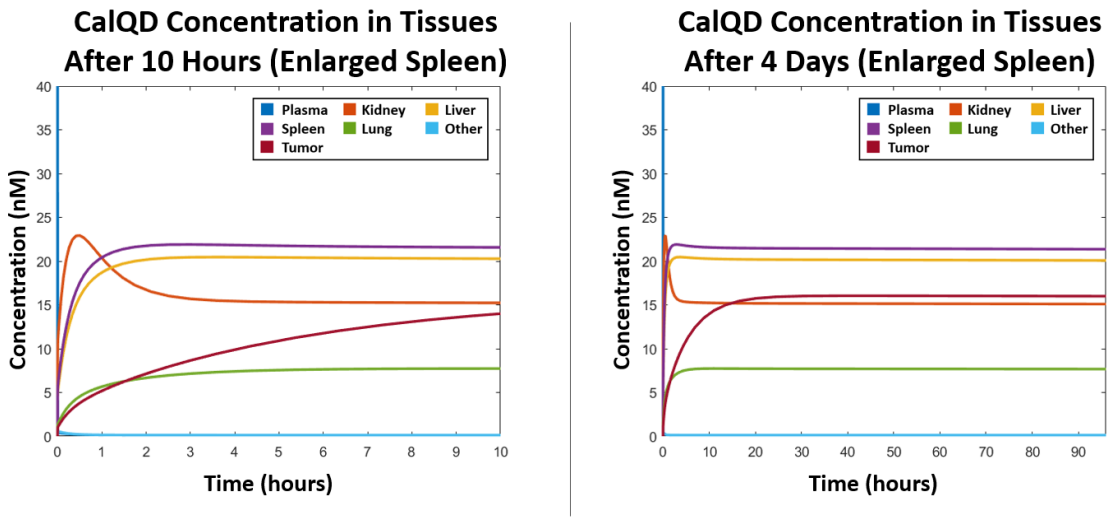

Figure 23. CalQD treatment time-concentration data for tumor-bearing mice in each tissue region in the case on an enlarged spleen after 10 hours (left) and 4 days (right).

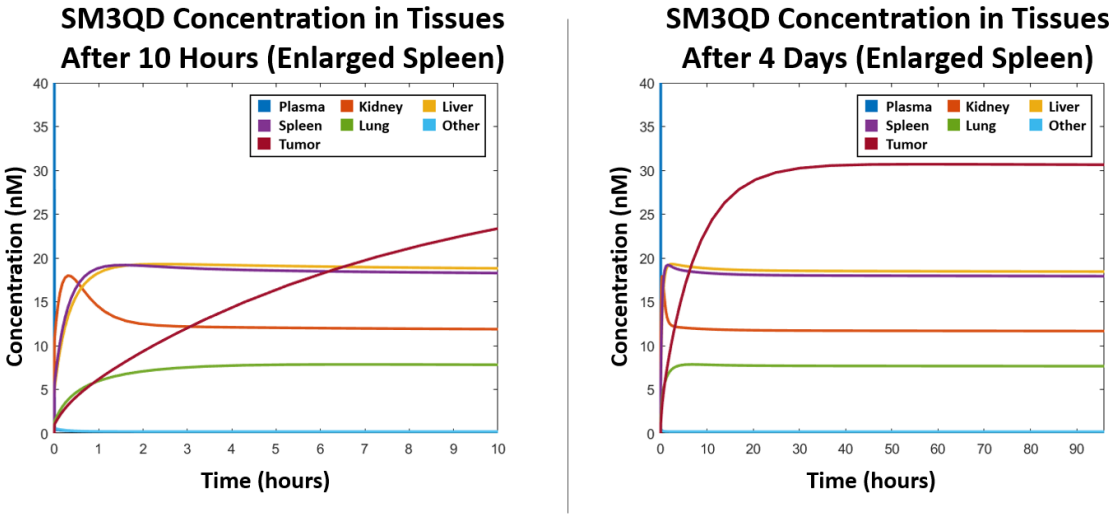

Figure 24. SM3 CalQD treatment time-concentration data for tumor-bearing mice in each tissue region in the case on an enlarged spleen after 10 hours (left) and 4 days (right).